Atmos. Chem. Phys. Discuss., 10, 30129–30170, 2010
www.atmos-chem-phys-discuss.net/10/30129/2010/
doi:10.5194/acpd-10-30129-2010
© Author(s) 2010. CC Attribution 3.0 License.

Atmospheric Chemistry and Physics Discussions

This discussion paper is/has been under review for the journal Atmospheric Chemistry and Physics (ACP). Please refer to the corresponding final paper in ACP if available.

Vertical profiles of nitrous acid in the nocturnal urban atmosphere of Houston, TX

K. W. Wong[1], H.-J. Oh[1], B. Lefer[2], B. Rappenglück[2], and J. Stutz[1]

[1]University of California Los Angeles, Department of Atmospheric and Oceanic Sciences, Los Angeles, CA 90095, USA
[2]Department of Earth and Atmospheric Science, University of Houston, Houston, TX 77204–5007, USA

Received: 27 November 2010 – Accepted: 29 November 2010
– Published: 10 December 2010

Correspondence to: J. Stutz (jochen@atmos.ucla.edu)

Published by Copernicus Publications on behalf of the European Geosciences Union.

Abstract

Nitrous acid (HONO) often plays an important role in tropospheric photochemistry as a major precursor of the hydroxyl radical (OH) in early morning hours and potentially during the day. However, the processes leading to formation of HONO and its vertical distribution at night, which can have a considerable impact on daytime ozone formation, are currently poorly characterized by observations and models. Long-path differential optical absorption spectroscopy (LP-DOAS) measurements of HONO during the 2006 TexAQS II Radical and Aerosol Measurement Project (TRAMP), near downtown Houston, TX, show nocturnal vertical profiles of HONO, with mixing ratios of up to 2.2 ppb near the surface and below 100 ppt aloft. Three nighttime periods of HONO, NO_2 and O_3 observations during TRAMP were used to perform model simulations of vertical mixing ratio profiles. By adjusting vertical mixing and NO_x emissions the modeled NO_2 and O_3 mixing ratios showed very good agreement with the observations.

Using a simple conversion of NO_2 to HONO on the ground, direct HONO emissions, as well as HONO loss at the ground and on aerosol, the observed HONO profiles were reproduced well by the model. The unobserved increase of HONO to NO_2 ratio ($HONO/NO_2$) with altitude that was simulated by the initial model runs was found to be due to HONO uptake being too small on aerosol and too large on the ground. Refined model runs, with adjusted HONO uptake coefficients, showed much better agreement of HONO and $HONO/NO_2$ for two typical nights, except during morning rush hour, when other HONO formation pathways are most likely active. One of the nights analyzed showed increase of HONO mixing ratios together with decreasing NO_2 mixing ratios that the model was unable to reproduce, most likely due to the impact of weak precipitation during this night.

HONO formation and removal rates averaged over the lowest 300 m of the atmosphere showed that NO_2 to HONO conversion on the ground was the dominant source of HONO, followed by traffic emission. Aerosol did not play an important role in HONO formation. Although ground deposition was also a major removal pathway of HONO,

ACPD
10, 30129–30170, 2010

net HONO production at the ground was the main source of HONO in our model studies. Sensitivity studies showed that in the stable NBL, net HONO production at the ground tends to increase with faster vertical mixing and stronger emission. Vertical transport was found to be the dominant source of HONO aloft.

1 Introduction

Nitrous acid, HONO is one of the most important hydroxyl radical (OH) precursors in the troposphere, in particular in environments with larger NO_x levels. Its photolysis (R1)

$$HONO + h\nu\ (\lambda < 400\ nm) \longrightarrow OH + NO \qquad (R1)$$

produces OH much earlier in the day than photolysis of O_3 and formaldehyde (HCHO). HONO photolysis is thus the dominant primary OH source in the morning. Low levels of HONO can also considerably contribute to the OH budget later during the day. The contribution of HONO photolysis to the total OH budget during the day can reach up to 34% in urban and rural environments (Acker et al., 2006; Kleffmann et al., 2005; Aumont et al., 2003; Alicke et al., 2002).

Despite the importance of HONO, its formation mechanism is yet not well understood. At night, when photolysis ceases, HONO mixing ratios increase gradually, reaching up to hundreds of ppt in rural areas and up to several ppb in polluted urban boundary layers (Stutz et al., 2010a; Kleffmann et al., 2006; Lammel and Cape, 1996; Platt, 1985). Different HONO formation pathways in urban areas have been identified as being important (Fig. 1). HONO is emitted directly into the atmosphere through combustion processes. Emissions depend on the type of engines and fuel, ranging from <0.01% to 1.8% of NO_x (Kurtenbach et al., 2001; Calvert et al., 1994; Pitts et al., 1984; Kessler and Platt, 1984). $HONO/NO_x$ emission ratios from traffic tunnels in California and Europe have been measured from 0.29% to 0.8% depending on the traffic density and the type of vehicles (Kurtenbach et al., 2001; Kirchstetter et al., 1996).

ACPD
10, 30129–30170, 2010

In the nocturnal boundary layer (NBL), HONO can also be formed in gas-phase and heterogeneous chemical reactions. The most significant gas-phase reaction that leads to HONO formation is the reaction of NO with OH.

$$NO + OH \xrightarrow{M} HONO \quad \text{(R2)}$$

This reaction is not significant during the night due to the low OH concentrations. Various other gas-phase HONO formation processes have been discussed and proposed in the past decades (Finlayson-Pitts et al., 2003; Li et al., 2008). However, none of these reactions is considered to be important at night.

It is currently believed that heterogeneous processes involving conversion of NO_2 on humid surfaces are the major formation pathways of nocturnal HONO as described by the following stoichiometry.

$$2NO_{2\,(g)} + H_2O_{\,(surface)} \longrightarrow HONO_{\,(g)} + HNO_{3\,(surface)} \quad \text{(R3)}$$

Laboratory studies show that HONO formation has a first order dependence on NO_2 and depends on relative humidity (Finlayson-Pitts et al., 2003; Kleffmann et al., 2004; Lammel and Cape, 1996). Other heterogeneous reactions such as NO + NO_2 + $H_2O \longrightarrow 2HONO$, reaction of NO and HNO_3 on silica surfaces in the presence of water, heterogeneous conversion of NO_2 and other reactions such as on soot surfaces appear to play only a minor role in HONO formation (Saliba et al., 2001; Calvert et al., 1994; Ammann et al., 2005; Gutzwiller et al., 2002; Arens et al., 2001; Kalberer et al., 1999; Kleffmann and Wiesen, 2005). A recent study by Ziemba et al. (2010) proposed that heterogeneous reaction of HNO_3 on fresh organic aerosol can be a potentially significant source of HONO. Photoenhanced sources of HONO from reaction of NO_2 on organic surfaces such as aromatic hydrocarbons and humic acids have been proposed (Stemmler et al., 2006; George et al., 2005) but will not be further discussed in this paper.

ACPD
10, 30129–30170, 2010

While direct emissions of HONO predominantly occurs near the surface, i.e. emissions by traffic, heterogeneous conversion of NO_2 to HONO can occur either on the ground and other surfaces such as buildings, plants etc, or on particles. In the former case one would expect clear vertical gradients of HONO, in particular during the night, when mixing is inefficient. In the case of NO_2 to HONO conversion on particles the vertical profile of HONO would follow the profile of the particles surface area, and would most likely lead to much weaker profiles. It is thus clear that the observation and interpretation of vertical concentration profiles at night can give crucial information on the nature of the surface responsible for the formation of HONO. Few attempts to use this information have been published thus far. Vertical gradients of HONO in the lowest 4 m altitude and fluxes of HONO were measured using differential optical absorption spectroscopy (DOAS) by Stutz et al. (2002) in a polluted rural area in Italy in 1998. Measurements showed that the compensation point for formation and deposition of HONO on grass surface occurred at HONO/NO_2 of ~0.03, and that emission was a significant source of HONO in polluted areas (Stutz et al., 2002). Kleffmann et al. (2003) performed HONO gradients measurement between 10–190 m altitudes in a semi-rural area in Germany in 2001. Their study showed that HONO formation was dominated by processes on ground surfaces and HONO formation on aerosol surface was insignificant (Kleffmann et al., 2003).

Knowledge of the vertical profiles of HONO is also crucial to quantify its nocturnal budget and its contribution to the HO_x budget in the morning. Here we present continuous measurements of vertical concentration profiles of HONO, NO_2 and O_3 in Houston, TX in 2006, with a focus on nighttime data. By using a 1-D chemistry and transport model, the observations will be interpreted to determine the surfaces responsible for HONO formation and to test whether simple model parameterizations of NO_2 to HONO conversion can explain the observations.

ACPD
10, 30129–30170, 2010

2 Experimental

During the Texas Air Quality Study (TexAQS) II Radical and Aerosol Measurement Project (TRAMP) in summer 2006, measurements of HONO, O_3, NO_2 and other trace gases were made from 15 August to 20 September in downtown Houston, using UCLA's long-path differential optical absorption spectroscopy (LP-DOAS) instrument.

The LP-DOAS instrument was set up on the roof of the North Moody Tower on the University of Houston campus, at an altitude of about 70 m above the ground. The LP-DOAS instrument sent a collimated beam of light from a Xe-arc lamp through a 1.5 m double Newtonian telescope. Three retroreflectors were mounted on the tops of three buildings (Toyota Center, El Paso Energy Building and JP Morgan Chase Tower) located in downtown Houston at distances of 4.1 km, 5.05 km and 5.15 km from the Moody Tower at altitudes of 20 m, 130 m and 300 m respectively (Fig. 2). The LP-DOAS telescope aimed consecutively at these retroreflectors in order to measure the absorptions of HONO, NO_2, and O_3, between the University of Houston and downtown Houston. Details of the LP-DOAS instrument can be found in Alicke et al. (2002); Stutz et al. (2010a,b) and Platt and Stutz (2008). The retrieved concentrations are horizontally averaged between the Moody Tower and downtown Houston and vertically averaged between the LP-DOAS height intervals(lower: 20–70 m, middle: 70–130 m and upper: 130–300 m) and are representative concentrations for the boxes shown in Fig. 2. The uncertainties of the NO_2, O_3, and HONO absorption cross sections are ± 5%, ± 3%, and ± 5%, respectively (Voigt et al., 2001; Stutz et al., 2002; Voigt et al., 2002). The systematic error of the DOAS spectrometer was determined to be <3% (Stutz and Platt, 1996). The observed mixing ratio ranges and detection limits are shown in Table 1. Information on supplemental measurements during TRAMP can be found in Lefer and Rappenglück (2010).

ACPD
10, 30129–30170, 2010

3 Observations

During the measurement period from 15 August to 20 September in 2006 during TRAMP, the best data on all three light paths were obtained during the first two weeks of September (1–14 September). Therefore, the discussion below is focused on this period (Fig. 3). All three trace gases established vertical gradients at night which disappeared in the morning when the boundary layer became well-mixed.

3.1 Meteorology

In-situ measurements of meteorological data, such as wind, temperature and relative humidity were recorded at the top of Moody Tower during the experiment. Wind speed and direction and relative humidity data are plotted in Fig. 3. During the measurement period from 1 to 14 September 2006, the prevailing winds were mostly northeasterly, with an averaged wind speed of ~3 m/s. At night, winds tended to be weaker than during the day, with an average of 2.5 m/s. However, wind directions were mostly northeasterly or southeasterly. Relative humidity during these two weeks ranged from 20% to 90%, with, in general, larger relative humidity at night. Details of the meteorology condition during TRAMP are discussed in Lefer et al. (2010).

3.2 NO_2 and O_3

NO_2 developed negative gradients during the night, with larger mixing ratios near the ground and smaller aloft, while positive gradients of O_3 were typically observed. This is due to the suppression of vertical mixing at night and NO emissions from traffic at the surface that converts O_3 to NO_2 as shown in Reaction 4. These gradient measurements are consistent with previous field observations (Wang et al., 2006; Stutz et al., 2004b).

$$NO + O_3 \longrightarrow NO_2 + O_2 \quad \text{(R4)}$$

ACPD
10, 30129–30170, 2010

During stable and polluted nights (1–2, 2–3, 6–7, 7–8 and 11–12 September), NO_2 mixing ratios at lower height interval reached above 40 ppb while NO_2 mixing ratios in the upper height interval were ~1 ppb or less. Difference of NO_2 mixing ratios between lower and upper height intervals reached up to 50 ppb, as observed on 7 September at 04:30 a.m.

O_3 mixing ratios in the lower height interval decreased throughout the night and were often below 20 ppb. O_3 mixing ratios decreased to below a few ppb during several nights (1–2, 2–3, 6–7, 7–8, 10–11, and 11–12 September). During these nights, O_3 mixing ratios in the upper height interval remained almost constant throughout the night. Difference of O_3 mixing ratios between lower and upper light paths exceeded 50 ppb on 2 and 7 September.

3.3 HONO

During the night, HONO generally followed the trend of NO_2 in all three height intervals. Negative vertical gradients were observed during the night, with larger concentrations near the ground and smaller aloft, similar to previous observations (Wang et al., 2006; Stutz et al., 2002; Kleffmann et al., 2003). Maximum nighttime HONO mixing ratios of 2 ppb and above were observed in the lower height interval on 1–2, 7–8 and 11–12 September. Difference of HONO mixing ratios between the lower and upper height intervals reached up to 1.5 ppb during the nights of 1–2, 6–7, 7–8, 10–11 and 11–12 September.

3.3.1 Selected polluted nights (1–2, 7–8 and 11–12 September)

Three periods (1–2, 7–8 and 11–12 September) with distinct vertical gradients (Figs. 4a, 5a, 6a) were selected for a more detailed analysis. 1–2 and 7–8 September had similar nocturnal variations of NO_2, HONO and O_3 with other nights. Vertical gradients of all three trace gases started to develop after sunset and became strongest towards the end of the night. Strong positive gradients of O_3 and negative gradients

ACPD
10, 30129–30170, 2010

of NO_2 were observed. O_3 at lower levels became depleted at the end of both nights, while the upper light path showed almost constant mixing ratios of about 60 ppb and 70 ppb throughout the nights. Based on the vertical trace gas profiles, temperature profiles (Day et al., 2010) and the results from our previous NO_3 lifetime analysis (Stutz et al., 2010b) we believe that the upper height interval was in the residual layer during both nights. HONO mixing ratios at all three levels, lower, middle and upper, were positively correlated with NO_2. Nighttime HONO concentrations were largest about an hour before sunrise and reached 2.15 ppb on 2 September and 2 ppb on 8 September in the lower height interval. During both nights, HONO mixing ratios in the upper height interval remained below 0.1 ppb. Differences in HONO mixing ratios between the lower and upper light paths reached 2.0 ppb and 1.7 ppb during the night of 1–2 and 7–8 September respectively. The main difference between these two nights is that HONO and NO_2 mixing ratios in the lower height interval reached their maximum at the same time during the night of 1–2 September, but NO_2 peaked an hour earlier than HONO during the night of 7–8 September.

The night of 11–12 September showed a very different picture. HONO and NO_2 mixing ratios at the lower light path did not follow each other closely as was typically observed during other nights. Instead, NO_2 in the lower height interval decreased throughout the night, while HONO accumulated. However, HONO in the middle and upper interval showed a positive correlation with NO_2. Differences in HONO mixing ratios between the lower and upper light paths reached 1.9 ppb. In addition, vertical gradients of O_3, HONO and NO_2 were observed already at the beginning of this night, while they were well-mixed at the beginning of the nights of 1–2 and 7–8 September and. This indicated the atmosphere was already stable before sunset.

Following the idea that the HONO to NO_2 ratios allow further analysis of NO_2 to HONO conversion (Stutz et al., 2004a) we also calculated this ratio (Fig. 4a, 5a, 6a). $HONO/NO_2$ was about 1–2% at the beginning of all three nights. $HONO/NO_2$ tended to be slightly larger at lower levels than aloft. There were no significant vertical gradients of the ratio except on 11–12 September, during the last few hours of the night. At the

ACPD
10, 30129–30170, 2010

lower level, the ratios increased throughout the night and reached a maximum of 4% and 6% respectively on 2 September and 12 September at the end of the night when HONO reached a maximum. On 7–8 September, HONO/NO_2 increased to 4% before midnight then was 3–4% throughout the night. Compared with results from Stutz et al. (2004a), the HONO/NO_2 during TRAMP seems to be lower. While HONO/NO_2 of up to 9% were observed in various field experiments as reported in Stutz et al. (2004a), a maximum ratio of 7% was measured during TRAMP. It should be noted here that the values reported by Stutz et al. (2004a) were corrected for direct emission of HONO and are thus expected to be larger. For a better comparison with the model we will use directly observed and modeled HONO/NO_2, without any further correction.

4 Model description

To further understand the HONO field measurements taken during TRAMP 2006, we used a 1-D Radical Chemistry and Transport model (RCAT8.2). RCAT8.2 includes the gas-phase Regional Atmospheric Chemistry Mechanism (RACM) and 84 reactive species and 244 gas phase chemical reactions (Stockwell et al., 1997). RCAT8.2 considers temporally varying anthropogenic emissions, predominately from traffic between 0.1 m and 1 m altitude, as well as biogenic emissions at the ground and between 1 m and 10 m altitude. Emission ratios used in the model are based on (Kurtenbach et al., 2002, 2001). Surface uptake resulting in dry deposition and chemistry on aerosol are included as well. Chemistry in the liquid phase is currently not considered in the model. Details of the model are described in Geyer and Stutz (2004a) and Wong and Stutz (2010).

ACPD
10, 30129–30170, 2010

4.1 Model setup

The model subdivides the lowest 2 km into 26 boxes (center of boxes at (m): 5×10^{-5}, 5.5×10^{-4}, 5.5×10^{-3}, 5.5×10^{-2}, 0.55, 2, 4.5, 8, 15, 27.5, 42.5, 60, 80, 100, 120, 140, 162.5, 187.5, 250, 400, 625, 875, 1125, 1375, 1625, 1975, 2500). Box heights decrease logarithmically below 1 m to take into account the inefficient vertical transport near the ground. An additional box from 2 km to 3 km is the upper boundary of the model. Vertical exchange of trace species between adjacent boxes occurs through turbulent diffusion as chemical reactions take place simultaneously at all altitudes.

4.2 Parameterization of HONO chemistry

In RCAT8.2 HONO is directly emitted from cars with emission ratio HONO/NO_x = 0.008 between 0.1–1 m altitude based on the tunnel measurement from Kurtenbach et al. (2001). Chemical HONO reactions currently included in the model include HONO photolysis (R1), the HONO reaction with OH and the formation of HONO from NO and OH (R2).

HONO is formed from conversion from NO_2 on aerosol and ground surfaces, with a yield of 50% following the stoichiometry of R3 and a NO_2 reactive uptake coefficient of 10^{-5} (Trick, 2004). Deposition rates of HONO and NO_2 are calculated by the number of molecules in the lowest box colliding with the ground and the uptake coefficient. The uptake rate of HONO and NO_2 on aerosols is determined from the aerosol surface area density and the uptake coefficients according to the mass-transfer equation given by (Fuchs and Sutugin, 1971) assuming an average particle diameter of 150 nm.

HONO is taken up on aerosol and ground surfaces with a reactive uptake coefficient 10^{-4} (Trick, 2004). The ground is assumed to be flat in the model and no buildings or trees were considered. Vertical transport of HONO, i.e. vertical HONO flux j_{HONO} is calculated based on a flux-gradient relationship and eddy diffusivity (Eq. 1) (Geyer and Stutz, 2004a). Eddy diffusivity is calculated by the Monin-Obukhov theory with

ACPD
10, 30129–30170, 2010

the Von Kármán constant κ, the friction velocity u^* and the stability correction factor Φ which is a function of altitude and stability through the Monin-Obukhov length L (Businger et al., 1971).

$$j_{\mathrm{HONO}}(z,t) = -K(z,t)\cdot\frac{\partial \mathrm{HONO}(z,t)}{\partial z}, \text{where } K(z,t) = \frac{\kappa\cdot u^*(t)\cdot z}{\Phi(\frac{z}{L},t)} \quad (1)$$

4.3 Model initialization

The model was initialized with a well-mixed boundary layer, using observed concentrations after sunset at 06:30 p.m. CST on 1 September and 7 September (Table 2). For the period of 11–12 September, the model was initialized with the observed vertical profiles of NO_2, HONO and O_3 and a stable boundary layer (Table 2). Because vertical gradients of other trace gases such as SO_2 and HCHO did not show vertical gradients at this time and, all trace gases except NO_2, HONO and O_3 were initialized with a constant vertical profile for this night. Typical volatile organic compounds (VOC) concentrations, constant at all heights, were used in all three model runs.

As previously described in Geyer and Stutz (2004a) nocturnal vertical profiles of most trace gases, and in particular O_3 and NO_x, depend strongly on two factors: vertical stability and NO_x emission rates. Both parameters are not known well enough for the TRAMP data to allow an accurate modeling of nocturnal chemistry. To ensure that we describe these two factors correctly before we attempt to simulate HONO profiles we adjusted NO_x emission rates and vertical mixing at each hour to make the modeled temporal and vertical profiles of NO_2 and O_3 fit the measurement. Vertical mixing was adjusted indirectly by varying the Monin-Obukhov length, which was used to calculate the eddy diffusivity. It should be noted here that the model was not constrained by any observed trace gas concentrations after initialization. HONO profiles were then calculated based on the adjusted emissions and stability parameters using the chemistry described above. No attempt to adjust the model to the HONO observations was made.

ACPD
10, 30129–30170, 2010

4.4 Applicability of 1-D Model

One of the obvious challenges in our approach is the use of a 1-D model that may have difficulties in situations where advection plays a role. Emissions from point-sources pose another obstacle for the 1-D model. However, unlike many previous comparisons between observations and model results our 1-D model was used to understand path-averaged LP-DOAS data. These observations were horizontally integrated over 4–5 km and vertically integrated over altitudes of 20–70 m, 70–130 m and 130–300 m. Therefore, any local effects such as freeways and small scale trace gas transport will be averaged and play a much smaller role than in comparisons with in-situ data.

The DOAS measurements are also representative for much larger areas. In Houston the light paths spanned approximately from downtown to the southern edge of the inner ring of Houston, bounded by Freeway 610 (Fig. 2). Since the Houston inner ring consists of urban and suburban areas with similar characteristics, the LP-DOAS observations should also be representative for the rest of the Houston inner ring.

4.4.1 Lateral transport

To investigate how trace gas advection could impact our modeling studies, we compared the vertical mixing timescale in the model with the observed horizontal transport timescales. The vertical mixing timescale in the model is calculated as $\tau_z(z,t) = \frac{z}{\kappa \cdot u^*(t)}$, where z is the altitude, κ is the Von Kármán constant and u^* is the friction velocity. The horizontal timescale was determined using the measured wind speed and assuming that our LP-DOAS measurements are representative for the Houston inner ring with ~20 km diameter. The 1-D model can be used if the vertical mixing timescale is much less than the horizontal timescale, i.e. $\tau_z \ll \tau_x$. In this case concentration changes due to advection are less than those caused by vertical transport and trace gases distribution in the lower atmosphere is governed by vertical transport rather than lateral transport. The comparison between the vertical and horizontal timescales showed that our 1-D model can be used to simulate the lower and the middle height intervals.

ACPD
10, 30129–30170, 2010

However, care has to be taken in the interpretation of the model calculations of the upper interval (130–300 m) as advection may potentially play a role. This is in agreement with a previous study (Stutz et al., 2010b) that concluded that the upper height interval was frequently in the residual layer in Houston.

4.4.2 Point emission

Another challenge in the use of the 1-D model is the upwind point emissions, for example from the petrochemical complex in the Houston ship channel area east of our measurement site. During easterly winds these emissions, which would be inhomogeneously distributed in the atmosphere, could reach our light paths. However, in-situ wind speed and direction measured at 70 m altitude at Moody Tower and radiosonde profiles (Day et al., 2010) showed that wind directions were not easterly during the three modeling periods and thus there was no significant influence of the ship channel emissions on our data. The only exception is 7–8 September between 03:30 a.m. to 04:00 a.m. CST in the lower and middle height intervals when an increase of about 10 ppb of NO_2 and 0.5 ppb of HONO in the lower interval, and a slight increase of NO_2 and HONO in the middle interval occurred. For our study we will thus treat the Houston inner ring as a metropolitan area where traffic is the dominant source of NO_x and HONO emission (Fig. 2).

4.5 Sensitivity to emission and vertical mixing

Sensitivity studies based on the model run of 1–2 September were performed to investigate the dependence of NO_2 and O_3 mixing ratios on NO_x emission and vertical mixing (Fig. 7). NO_x emission, adjusted to yield agreement with the observations, showed the evening rush hours in the first few hours of the model runs, followed by low emissions throughout the night until the onset of the morning rush hours. Similar emission patterns were found in the modeling periods of 7–8 and 11–12 September. Variation of eddy diffusivity, also adjusted for best agreement between modeled NO_2

ACPD
10, 30129–30170, 2010

and O_3, showed that the boundary layer was weakly stable during the first two hours and stable throughout the rest of the night. Similar eddy diffusivities were used during the night of 7–8 September. 11–12 September had a less stable boundary layer since observations showed some mixing between the lower and middle height intervals.

NO_2 mixing ratios in the lower height intervals were very sensitive to changes in NO_x emissions. A change of 20% in NO_x emissions in the model run will lead to a significant change in modeled NO_2 mixing ratios. Sensitivity of NO_2 to NO_x emissions decreases with altitude. As shown in Fig. 7, an uncertainty of +/− 20% in the NO_x emission rates seems to capture the disagreement between the best modeled NO_2 mixing ratio and the observations on both light paths throughout the night. NO_2 concentrations did not seem to be very sensitive to variations in eddy diffusivity. However, eddy diffusivity values were small during the night. Thus changes of eddy diffusivity adopted in the sensitivity runs did not make a significant change in the stability or vertical mixing of the boundary layer. Sensitivity of NO_2 to eddy diffusivity also decreases with altitudes.

The sensitivity runs also show that our method of adjusting NO_x emissions and vertical mixing seems to yield reasonable and fairly accurate results. We thus conclude that the adjusted NO_x emissions and vertical mixing parameters provide accurate input parameters for our model runs to study HONO chemistry.

5 Modeling results

Model results for 1–2, 7–8 and 11–12 September are shown in Figs. 4b, 5b, 6b. For a better comparison with the observations we integrated the mixing ratios from the model over the three observational height intervals, i.e. lower (20–70 m), middle (70–130 m) and upper (130–300 m).

5.1 NO_2 and O_3

The modeled NO_2 and O_3 mixing ratios for all three nights (1–2, 7–8 and 11–12 September,) agree well with the observations, except for NO_2 in the upper height

ACPD
10, 30129–30170, 2010

interval which tends to be larger than the measurements on 1–2 and 7–8 September. Because the upper height interval was most likely in the residual layer during these nights, the weak mixing into the residual layer and/or the possible air mass exchange above 130 m was not simulated accurately in the model. On 11–12 September, mixing of NO_2 at the lower and middle height intervals occurred in the second half of the night. This was simulated until the two were well-mixed, but the modeled NO_2 again developed gradients while the observed NO_2 between the lower and middle light path intervals remained well-mixed.

5.2 HONO

The modeled HONO mixing ratios and profiles showed good agreement with the observations for 1–2 and 7–8 September, except for the last few hours of the night when HONO was under-predicted by the model. HONO mixing ratios in the upper height interval were greater in the model than the observations, as the upper height interval was often located in the residual layer. The elevated HONO at this altitude was probably due to an overestimate of vertical mixing into the residual layer by the model and/or transport processes in the residual layer which are not represented well in the model.

Comparison of HONO/NO_2 from the model with the observations allows further analysis of the HONO formation processes and their altitude dependence. Our model calculation showed a surprising increase of HONO/NO_2 with altitude on 1–2 and 7–8 September, which was not reflected in the observations. This suggested that there was either too little NO_2 and/or too much HONO in the middle and upper altitude intervals in the model. Sensitivity studies revealed that increasing NO_2 in the model leads to NO_3 and N_2O_5 mixing ratios which were considerably larger than the observations (Stutz et al., 2010b). We thus concluded that the increase of HONO/NO_2 aloft was due to excess HONO instead of the lack of NO_2. Attempts to decrease the HONO/NO_2 at middle and upper altitudes by adjusting the uptake coefficients of NO_2 and/or the conversion factor of NO_2 were not successful. Further analysis of HONO chemistry showed that the elevated HONO/NO_2 was most likely due to an underestimate of the

ACPD
10, 30129–30170, 2010

loss of HONO on the aerosol. Modeled HONO/NO_2 in the lower height interval for the three periods was slightly lower than the observations, indicating that HONO is formed at the ground more efficiently than implemented in our original model. Sensitivity studies showed that the underestimated HONO/NO_2 at lower altitude interval is due to the excess loss of HONO by deposition on the ground.

To consider the excess loss of HONO at the ground and the inadequate loss of HONO on aerosol in the model, refined model runs were carried out in which the HONO uptake coefficient at the ground was decreased by a factor of five to 2×10^{-5}, while the HONO uptake on the aerosol was increased ten times to 10^{-3}. In our original model runs HONO uptake coefficients on aerosol and ground were 10^{-4}, based on measurements on asphalt by Trick (2004). In reality, the uptake coefficients are likely to be different on aerosol and ground. HONO uptake coefficients on the order of 10^{-4} to 10^{-2} were reported by several studies (Yu et al., 2009). HONO uptake coefficients on sulfate particles on the order of 10^{-3} were reported by Harrison and Collins (1998). The HONO uptake coefficient used in our refined model runs thus seems to be within the range of published values.

The refined model results (Figs. 4c, 5c, 6c) showed an increase of HONO mixing ratios at lower altitudes in all three runs compared to the original modeled results, leading to a better agreement between model and observations. There is no change in the modeled NO_2 and O_3 mixing ratios in the refined model runs. On 1–2 September, the modeled HONO/NO_2 in the lower and middle height intervals agreed very well with the observations until the last few hours of the night when the observed HONO mixing ratios increased and peaked. The observed HONO/NO_2 reached 5% while the modeled ratio was only 2.5%. This was most likely due to a process that leads to large HONO/NO_2 such as HNO_3 conversion on fresh soot aerosol observed by Ziemba et al. (2010) during rush hour.

On 7–8 September, the modeled HONO in the lower height interval was slightly smaller in the middle of the night, but it showed a good agreement with the observations during the last few hours of the night. HONO reached a maximum of 1.7 ppb in

ACPD
10, 30129–30170, 2010

the model while the observed mixing ratio was 2 ppb. $HONO/NO_2$ in the lower height interval was better predicted on 7–8 Septenber in the refined model run. In both modeling periods, the HONO mixing ratios at upper altitude intervals were larger than the observations as the upper light path was located in the residual layer which was not captured accurately by the model.

In general, the refined model improved the agreement between model and observations on 1–2 and 7–8 September. However, the model was not able to reproduce the opposite temporal behavior of HONO and NO_2 in the lower height interval during the night of 11–12 September. The modeled HONO mixing ratios in the lower height interval remained constant at about 0.7 ppb and decreased slightly towards the end of the night while the observed HONO increased steadily throughout the night to 2 ppb at the end of the night. In addition, the modeled $HONO/NO_2$ remained almost constant at around 2% throughout the night and did not predict the increase of $HONO/NO_2$ to 6%, as observed. This night differed in its behavior considerably from the other two. 11–12 September was the only night throughout the two weeks of measurements (Fig. 3) with opposite temporal behavior of HONO and NO_2. The decrease of NO_2 at the lower light path throughout the night was due to the low O_3 at the beginning of the night. As surface NO_2 is predominately formed from the reaction of ozone with NO (R4), the NO_2 surface source was small in this night. This interpretation is consistent with the very low NO_3 mixing ratio observations (not shown). It is not clear what caused the increase of HONO with decreasing NO_2 at lower altitude intervals. One possible explanation was the more efficient HONO formation at larger relatively humidity as reported by Stutz et al. (2004a), as this night was more humid than the other two. The average relatively humidity at 70 m was about 85% during this night and 70–75% during the other two periods. In addition, there was precipitation at the beginning of the night of 11–12 September according to the National Climate Data Center (http://www.ncdc.noaa.gov/oa/climateresearch.html). We therefore conclude that precipitation processes wetting the ground and other surfaces during the night of 11–12 September lead to substantially different HONO chemistry, which is currently not

ACPD
10, 30129–30170, 2010

implemented in the model. Because our model did not describe the HONO correctly, this night will not be further quantitatively analyzed below.

In the following we will focus on the refined model runs of 1–2 and 7–8 September, as the refined model runs describe the HONO chemistry better. To visualize the vertical mixing ratio profiles and their development throughout the night, the vertical profiles of HONO and NO_2 mixing ratios at 19:30, 00:30 and 05:30 CST were extracted from the model simulations for the two modeling periods, 1–2 and 7–8 September (Fig. 8). HONO slowly accumulated in the lowest 200 m of the atmosphere, with pronounced vertical mixing ratios profiles. Vertical HONO gradients, i.e. comparing 20 m to 300 m altitude, increased throughout the night with changes occurring mainly below 100 m, especially on 7–8 September. Most of the HONO was located in the lowest 200 m of the atmosphere. HONO mixing ratios below 20 m, which were not observed by the LP-DOAS, showed that HONO near the ground (at 0.55 m) increased from 1.8 ppb at 19:30 CST to 2.4 ppb at 00:30 CST and to 4.6 ppb at 05:30 CST during the night of 7–8 September. This is significantly larger than the modeled and observed values of the lower light path of 0.45 ppb at 19:30, 0.45 ppb at 00:30 CST and 1.7 ppb at 05:30 CST. The vertical profiles of HONO indicated that HONO near the ground (at 0.55 m) can be considerably larger than values from only 20–70 m above the surface. Consequently care has to be taken when extrapolating surface measurements of HONO to the entire boundary layer.

6 Discussion

Vertical profiles of HONO mixing ratios can give information on the nature of the surface responsible for the formation of HONO. Since HONO developed negative gradients throughout the night and its concentration increases near the ground throughout the night, one can interpret that the source of HONO is near or at the ground. It is however difficult to quantify the contributions of different HONO formation and loss processes and their altitude dependence based on vertical concentration profiles alone.

ACPD
10, 30129–30170, 2010

6.1 HONO rates profiles

To further understand HONO chemistry and to investigate which processes are important for HONO in the nocturnal boundary layer, modeled HONO formation and loss rates were computed and the vertical profiles of these rates were extracted for the model period of 1–2 September at 19:30, 00:30 and 05:30 CST (Fig. 9). The rate of change of HONO depends on several factors as shown in Eq. (2). HONO is formed at the ground and potentially also on aerosol surfaces from NO_2 conversion ($P_{ground} + P_{aerosol}$), emitted from traffic (E) and released through the reaction of NO and OH ($P_{NO+OH\rightarrow HONO}$). Vertical transport of HONO (Ψ) can be both a source and a sink. HONO in the nocturnal boundary layer can be lost through reaction with OH and deposition at the ground and uptake on aerosol surfaces ($L_{ground} + L_{aerosol}$).

$$\frac{d\mathrm{HONO}}{dt} = P_{ground} + P_{aerosol} + E + P_{NO+OH\rightarrow HONO} + L_{ground} + L_{aerosol} + L_{HONO+OH} + \Psi \qquad (2)$$

The rate profiles (Fig. 9) show that HONO formation and loss processes were largest at or near the ground. The dominant formation pathway of HONO was through NO_2 conversion at the ground, followed by direct HONO emission. HONO formation and uptake on aerosol surfaces occurred over the lowest 300 m with rates slowly increasing towards the ground, where NO_2 and HONO mixing ratios are largest, assuming that the aerosol profile was uniform over the NBL. The formation of HONO on aerosol played a less important role. The model predicted about $\sim 10^5$ cm^{-3} nocturnal OH from NO_3 reactions with VOCs and ozonolysis of alkenes near the surface (see also Geyer and Stutz, 2004b). Production of HONO through reaction of NO and OH thus mainly occurred in the lower nocturnal boundary layer where NO mixing ratios were largest and decreased strongly with altitude. HONO formation by reaction of NO and OH was a minor production pathway of HONO in the NBL.

Among all the loss pathways, ground deposition of HONO was the largest. Chemical removal of HONO by OH, which decreased exponentially with altitude, was negligible. HONO uptake on aerosol occurred over the lowest 300 m with rates increasing toward

ACPD
10, 30129–30170, 2010

the ground where HONO concentrations were largest but, averaged over the NBL, this process was not as large as removal HONO by ground deposition. Finally, HONO rate profiles showed that HONO vertical transport redistributed HONO over the boundary layer and in general transports HONO upward, leading to a loss of HONO near the ground and a gain of HONO at higher altitude. In all model runs, vertical transport was the dominant source of nocturnal HONO above 20 m altitude in average.

6.2 Integrated HONO production and loss

Nocturnal HONO formation and removal rates change significantly throughout the nights of the two modeling periods due to the changes of meteorological condition and traffic patterns. In order to quantify the overall contribution of each HONO formation and loss process, the integrated HONO production and loss process in the lowest 300 m throughout the night were calculated for 1–2 and 7–8 September (Table 3).

Vertically and nocturnally integrated HONO production ranged from 1.7×10^{15} cm^{-2} to 1.8×10^{15} cm^{-2} in the two modeling periods. Contribution to total HONO production was 65–74% by NO_2 conversion at the ground, 3% by NO_2 conversion on aerosol, 17–21% from traffic, and 6–21% from reaction of NO and OH. Integrated HONO loss ranged from 1.3×10^{15} cm^{-2} to 1.4×10^{15} cm^{-2}. Contribution of total HONO removal was 71–76% by ground deposition, 18% by aerosol uptake and 1% due to reaction of HONO with OH. Vertical transport redistributed HONO over the NBL and even the residual layer. Vertical transport to altitudes above 300 m contributed to 5–10% of total HONO loss in the lowest 300 m. Combining all the factors, the overall HONO net production was 2.7×10^{14} cm^{-2} throughout the night of 1–2 September and 5.3×10^{14} cm^{-2} for 7–8 September. Assuming that all the HONO formed at night photolyzed into NO and OH, these numbers represent the amount of additional OH being contributed by HONO photolysis to the OH budget in the following day. However, because the HONO mixing ratios in the model simulations were smaller than the observations during the last few hours of the night, the actual HONO formation during these two nights should have been even greater.

ACPD
10, 30129–30170, 2010

6.3 Dependence of net HONO formation at the ground on vertical stability and emission

As proposed in Stutz et al. (2002, 2004a) the HONO/NO_2 system tends towards reaching a pseudo steady state (PSS) between HONO formation and loss. One would expect that in our case the air close to the ground was in this PSS. Our model analysis, however, identified the ground as a net source of HONO during the majority of time. Consequently the system, and in particular the lowest box of our model was shifted away from the pseudo steady state by vertical mixing processes. One can thus expect that vertical mixing and emission both modulate the HONO to NO_2 ratio at the ground, HONO chemistry at the ground, and as a consequence also the integrated net HONO formation in the NBL.

Vertical mixing plays two roles for HONO chemistry at the ground. It controls the amount of NO_2 available for making HONO at the ground and transports newly formed HONO upwards, away from the ground thus affecting HONO ground deposition. For example, weaker vertical mixing in the NBL can lead to larger NO_2 and HONO at the ground and consequently HONO formation and deposition at the ground (Fig. 10). Sensitivity model runs with constant emission show that impact of vertical mixing on net HONO formation can be categorized into two regimes, "transport sensitive" and "NO_2 sensitive". The "transport sensitive" regime occurs when vertical mixing is weak (in this case when K_z at 10 m is less than 0.6 m^2/s) (Fig. 10). During this regime, when vertical mixing becomes stronger, the net formation at the ground increases because vertical mixing transports HONO upward more efficiently leading to a greater decrease in deposition at the ground. This effect outweighs the simultaneous decrease of both NO_2 and thus HONO formation at the ground due to mixing of NO_2 into larger volumes. On the other hand, the "NO_2 sensitive" regime occurs when vertical mixing is efficient (in this case when K_z at 10 m is greater than 0.6 m^2/s) and the reduction of HONO production due to decreased levels of NO_2 is more substantial than the decrease of HONO deposition due to larger transport. Therefore net HONO production decreases in this regime, i.e. when vertical mixing is stronger.

ACPD
10, 30129–30170, 2010

Sensitivity runs were also carried out to test the effect of emission strength of NO_x and HONO on HONO chemistry at the ground. Under the condition of constant nocturnal vertical mixing, when the emission is increased, the model shows an increase of both HONO formation and removal at the ground due to the increase of both HONO and NO_2, which leads to an increase of net HONO production at the ground. The opposite is true when emission decreases. Therefore, addition of HONO by direct emission leads to larger net HONO formation at the ground when vertical mixing is constant.

7 Conclusions

During two weeks of the TRAMP 2006 experiment in Houston, TX, (1–14 September, 2006) nocturnal vertical concentration gradients of HONO, NO_2 and O_3 were frequently observed by the LP-DOAS. HONO developed negative gradients with larger concentrations near the ground and smaller aloft. Maximum HONO mixing ratios of above 2 ppb were observed in the lower height interval (average 20–70 m) in the late night, while HONO was often below 100 ppt in the upper height interval (130–300 m). These observations thus indicate that care has to be taken in interpreting surface observations of HONO, as they are not representative for the entire nocturnal boundary layer.

Three nights (1–2, 7–8 and 11–12 September) were selected to perform modeling studies and compare to the observations. Our vertically highly resolved 1-D chemistry and transport model (RCAT 8.2) together with the parameterization of NO_2 to HONO conversion and HONO loss rate at the ground (Trick, 2004) reproduced the observed vertical concentration profiles of HONO, NO_2 and O_3. However, the modeled $HONO/NO_2$ in the middle (70–130 m) and upper (130–300 m) height intervals was substantial larger than the observations, resulting in an increase of $HONO/NO_2$ with altitude in the model, that was not observed in the atmosphere. Analysis of HONO chemistry in the model indicated that the uptake coefficients of HONO were too small on aerosol and too large on the ground. Refined model runs with 10 times larger HONO aerosol uptake (10^{-3}) and 5 times smaller ground uptake (2×10^{-5}) showed a much

ACPD
10, 30129–30170, 2010

better agreement of HONO/NO_2 with observations for 1–2 and 7–8 September. Better laboratory HONO uptake data is needed to confirm the validity of these uptake coefficients on urban surfaces and aerosol.

The HONO mixing ratios at lower and middle altitude intervals from the refined model showed very good agreement with the observations for 1–2 and 7–8 September, except during morning rush hour. The greater HONO/NO_2 observed during morning rush hour was most likely due to additional conversion from HNO_3 on organic aerosol, as proposed by Ziemba et al. (2010), which is currently not included in our model. The model was not capable of capturing the unusual behavior of HONO for 11–12 September, which was most likely caused by precipitation in this night significantly changing HONO formation or loss.

Vertical profiles of modeled HONO rates of the two periods (1–2 and 7–8 September) showed that NO_2 conversion on the ground was the largest source of HONO (65–74%), followed by emission (17–21%). NO_2 conversion on aerosol did not play a significant role in HONO formation in our model. On the other hand, deposition at the ground was also the major sink of HONO (71–76%), followed by uptake on aerosol (18%). In our modeling studies, the ground acted as both the largest source and sink of HONO in the NBL through NO_2 conversion and HONO deposition. There was a net production of HONO at the ground throughout the three modeling periods. Vertical transport played the dominant role as the source of HONO aloft. Sensitivity studies showed that HONO formation at the ground can be modulated by both vertical mixing and emission. In the stable NBL, net HONO production increases with stronger vertical mixing and stronger emission.

Acknowledgements. This study was supported by a Career Award from the National Science Foundation Atmospheric Chemistry Program (ATM-0348674), the Texas Environmental Research Consortium, and the Houston Advanced Research Center (Grants H78, H86, and H104C).

ACPD
10, 30129–30170, 2010

References

Acker, K., Moller, D., Wieprecht, W., Meixner, F., Bohn, B., Gilge, S., Plass-Dulmer, C., and Berresheim, H.: Strong daytime production of OH from HNO_2 at a rural mountain site, Geophys. Res. Lett., 33, L02809, doi:10.1029/2005GL024643, 2006. 30131

Alicke, B., Platt, U., and Stutz, J.: Impact of nitrous acid photolysis on the total hydroxyl radical budget during the Limitation of Oxidant Production/Pianura Padana Produzione di Ozono study in Milan, J. Geophys. Res., 107, 8196, doi:10.1029/2000JD000075, 2002. 30131, 30134

Ammann, M., Rossler, E., Strekowski, R., and George, C.: Nitrogen dioxide multiphase chemistry: Uptake kinetics on aqueous solutions containing phenolic compounds, Phys. Chem. Chem. Phys., 7, 2513–2518, 2005. 30132

Arens, F., Gutzwiller, L., Baltensperger, U., Gaggeler, H., and Ammann, M.: Heterogeneous reaction of NO_2 on diesel soot particles, Environ. Sci. Technol., 35, 2191–2199, 2001. 30132

Aumont, B., Chervier, F., and Laval, S.: Contribution of HONO sources to the $NO_x/HO_x/O_3$ chemistry in the polluted boundary layer, Atmos. Environ., 37, 487–498, 2003. 30131

Businger, J., Wyngaard, J., Izumi, Y., and Bradley, E.: Flux-profile relationships in atmospheric surface layer, J. Atmos. Sci., 28, 181–189, 1971. 30140

Calvert, J., Yarwood, G., and Dunker, A.: An evalutation of the mechanism of nitrous-acid formation in the urban atmosphere, Res. Chem. Intermediat., 20, 463–502, 1994. 30131, 30132

Day, B. M., Rappenglueck, B., Clements, C. B., Tucker, S. C., and Brewer, W. A.: Nocturnal boundary layer characteristics and land breeze development in Houston, Texas during TexAQS II, Atmos. Environ., 44, 4014–4023, doi:10.1016/j.atmosenv.2009.01.031, 2010. 30137, 30142

Finlayson-Pitts, B., Wingen, L., Sumner, A., Syomin, D., and Ramazan, K.: The heterogeneous hydrolysis of NO_2 in laboratory systems and in outdoor and indoor atmospheres: An integrated mechanism, Phys. Chem. Chem. Phys., 5, 223–242, doi:10.1039/b208564j, 2003. 30132

Fuchs, N. A. and Sutugin, A. G.: Highly dispersed aerosols, Ann Arbor Science, Ann Arbor, Mi, 1971. 30139

George, C., Strekowski, R., Kleffmann, J., Stemmler, K., and Ammann, M.: Photoenhanced uptake of gaseous NO_2 on solid-organic compounds: a photochemical source of HONO?,

ACPD
10, 30129–30170, 2010

Faraday Discuss., 130, 195–210, doi:10.1039/b417888m, 2005. 30132
Geyer, A. and Stutz, J.: Vertical profiles of NO_3, N_2O_5, O_3, and NO_x in the nocturnal boundary layer: 2. Model studies on the altitude dependence of composition and chemistry, J. Geophys. Res., 109, D16398, doi:10.1029/2003JD004211, 2004a. 30138, 30139, 30140
Geyer, A. and Stutz, J.: The vertical structure of OH-HO_2-RO_2 chemistry in the nocturnal boundary layer: A one-dimensional model study, J. Geophys. Res., 109, D16301, doi:10.1029/2003JD004425, 2004b. 30148
Gutzwiller, L., Arens, F., Baltensperger, U., Gaggeler, H., and Ammann, M.: Significance of semivolatile diesel exhaust organics for secondary HONO formation, Environ. Sci. Technol., 36, 677–682, doi:10.1021/es015673b, 2002. 30132
Harrison, R. and Collins, G.: Measurements of reaction coefficients of NO_2 and HONO on aerosol particles, J. Atmos. Chem., 30, 397–406, 1998. 30145
Kalberer, M., Ammann, M., Arens, F., Gaggeler, H., and Baltensperger, U.: Heterogeneous formation of nitrous acid (HONO) on soot aerosol particles, J. Geophys. Res., 104, 13825–13832, 1999. 30132
Kessler, C. and Platt, U.: Nitrous acid in polluted air masses - Sources and formation pathways, in: Physico-chemical Behaviour of Atmospheric Pollutants (Proceedings), edited by: Versino, B. and Angeletti, G., 412–422, D. Reidel, Dordrecht, 1984. 30131
Kirchstetter, T., Harley, R., and Littlejohn, D.: Measurement of nitrous acid in motor vehicle exhaust, Environ. Sci. Technol., 30, 2843–2849, 1996. 30131
Kleffmann, J. and Wiesen, P.: Heterogeneous conversion of NO_2 and NO on HNO_3 treated soot surfaces: atmospheric implications, Atmos. Chem. Phys., 5, 77–83, doi:10.5194/acp-5-77-2005, 2005. 30132
Kleffmann, J., Kurtenbach, R., Lorzer, J., Wiesen, P., Kalthoff, N., Vogel, B., and Vogel, H.: Measured and simulated vertical profiles of nitrous acid - Part I: Field measurements, Atmos. Environ., 37, 2949–2955, doi:10.1016/S1352-2310(03)00242-5, 2003. 30133, 30136
Kleffmann, J., Benter, T., and Wiesen, P.: Heterogeneous reaction of nitric acid with nitric oxide on glass surfaces under simulated atmospheric conditions, J. Phys. Chem. A, 108, 5793–5799, doi:10.1021/jp040184u, 2004. 30132
Kleffmann, J., Gavriloaiei, T., Hofzumahaus, A., Holland, F., Koppmann, R., Rupp, L., Schlosser, E., Siese, M., and Wahner, A.: Daytime formation of nitrous acid: A major source of OH radicals in a forest, Geophys. Res. Lett., 32, doi:10.1029/2005GL022524, 2005. 30131
Kleffmann, J., Lorzer, J., Wiesen, P., Kern, C., Trick, S., Volkamer, R., Rodenas, M., and

ACPD
10, 30129–30170, 2010

Wirtz, K.: Intercomparison of the DOAS and LOPAP techniques for the detection of nitrous acid (HONO), Atmos. Environ., 40, 3640–3652, doi:10.1016/j.atmosenv.2006.03.027, 2006. 30131

Kurtenbach, R., Becker, K., Gomes, J., Kleffmann, J., Lorzer, J., Spittler, M., Wiesen, P., Ackermann, R., Geyer, A., and Platt, U.: Investigations of emissions and heterogeneous formation of HONO in a road traffic tunnel, Atmos. Environ., 35, 3385–3394, 2001. 30131, 30138, 30139

Kurtenbach, R., Ackermann, R., Becker, K., Geyer, A., Gomes, J., Lorzer, J., Platt, U., and Wiesen, P.: Verification of the contribution of vehicular traffic to the total NMVOC emissions in Germany and the importance of the NO_3 chemistry in the city air, J. Atmos. Chem., 42, 395–411, 2002. 30138

Lammel, G. and Cape, J.: Nitrous acid and nitrite in the atmosphere, Chem. Soc. Rev., 25, 361–369, 1996. 30131, 30132

Lefer, B. and Rappenglück, B.: The TexAQS-II radical and aerosol measurement project (TRAMP) Preface, Atmos. Environ., 44, 3997–4004, doi:10.1016/j.atmosenv.2010.05.053, 2010. 30134

Lefer, B., Rappenglück, B., Flynn, J., and Haman, C.: Photochemical and meteorological relationships during the Texas-II Radical and Aerosol Measurement Project (TRAMP), Atmos. Environ., 44, 4005–4013, doi:10.1016/j.atmosenv.2010.03.011, 2010. 30135

Li, S., Matthews, J., and Sinha, A.: Atmospheric hydroxyl radical production from electronically excited NO_2 and H_2O, Science, 319, 1657–1660, doi:10.1126/science.1151443, 2008. 30132

Pitts, J., Biermann, H., Winer, A., and Tuazon, E.: Spectroscopic identification and measurement of gaseous nitrous-acid in dilute auto exhaust, Atmos. Environ., 18, 847–854, 1984. 30131

Platt, U.: The origin of nitrous and nitric acid in the atmosphere, in: Chemistry of Multiphase Atmospheric Systems, edited by: Jaeschke, W., 229–319, Springer, New York, 1985. 30131

Platt, U. and Stutz, J.: Differential Optical Absorption Spectroscopy: Principles and Applications, Springer, Berlin, Heidelberg, doi:10.1007/978-3-540-75776-4, 2008. 30134

Saliba, N., Yang, H., and Finlayson-Pitts, B.: Reaction of gaseous nitric oxide with nitric acid on silica surfaces in the presence of water at room temperature, J. Phys. Chem. A, 105, 10339–10346, doi:10.1021/jp012330r, 2001. 30132

Stemmler, K., Ammann, M., Donders, C., Kleffmann, J., and George, C.: Photosensitized re-

ACPD
10, 30129–30170, 2010

duction of nitrogen dioxide on humic acid as a source of nitrous acid, Nature, 440, 195–198, doi:10.1038/nature04603, 2006. 30132
Stockwell, W., Kirchner, F., Kuhn, M., and Seefeld, S.: A new mechanism for regional atmospheric chemistry modeling, J. Geophys. Res., 102, 25847–25879, 1997. 30138
Stutz, J. and Platt, U.: Numerical analysis and estimation of the statistical error of differential optical absorption spectroscopy measurements with least-squares methods, Appl. Opt., 35, 6041–6053, 1996. 30134
Stutz, J., Alicke, B., and Neftel, A.: Nitrous acid formation in the urban atmosphere: Gradient measurements of NO_2 and HONO over grass in Milan, Italy, J. Geophys. Res., 107, 8192, doi:10.1029/2001JD000390, 2002. 30133, 30134, 30136, 30150
Stutz, J., Alicke, B., Ackermann, R., Geyer, A., Wang, S., White, A., Williams, E., Spicer, C., and Fast, J.: Relative humidity dependence of HONO chemistry in urban areas, J. Geophys. Res., 109, D03307, doi:10.1029/2003JD004135, 2004a. 30137, 30138, 30146, 30150
Stutz, J., Alicke, B., Ackermann, R., Geyer, A., White, A., and Williams, E.: Vertical profiles of NO_3, N_2O_5, O_3, and NO_x in the nocturnal boundary layer: 1. Observations during the Texas Air Quality Study 2000, J. Geophys. Res., 109, D16398, doi:10.1029/2004JD005216, 2004b. 30135
Stutz, J., Oh, H.-J., Whitlow, S. I., Anderson, C., Dibbb, J. E., Flynn, J. H., Rappenglück, B., and Lefer, B.: Simultaneous DOAS and mist-chamber IC measurements of HONO in Houston, TX, Atmos. Environ., 44, 4090–4098, doi:10.1016/j.atmosenv.2009.02.003, 2010a. 30131, 30134
Stutz, J., Wong, K. W., Lawrence, L., Ziemba, L., Flynn, J. H., Rappenglück, B., and Lefer, B.: Nocturnal NO_3 radical chemistry in Houston, TX, Atmos. Environ., 44, 4099–4106, doi:10.1016/j.atmosenv.2009.03.004, 2010b. 30134, 30137, 30142, 30144
Trick, S.: Formation of nitrous acid on urban surfaces - a physical-chemical perspective, Ph.D. thesis, University of Heidelberg, Heidelberg, Germany, 2004. 30139, 30145, 30151
Voigt, S., Orphal, J., Bogumil, K., and Burrows, J. P.: The temperature dependence (203–293 K) of the absorption cross sections of O_3 in the 230–850 nm region measured by Fourier-transform spectroscopy, J. Photochem. Photobio. A, 143, 1–9, doi:10.1016/S1010-6030(01)00480-4, 2001. 30134
Voigt, S., Orphal, J., and Burrows, J.: The temperature and pressure dependence of the absorption cross-sections of NO_2 in the 250–800 nm region measured by Fourier-transform spectroscopy, J. Photoch. Photobio. A, 149, 1–7, 2002. 30134

ACPD
10, 30129–30170, 2010

Wang, S., Ackermann, R., and Stutz, J.: Vertical profiles of O_3 and NO_x chemistry in the polluted nocturnal boundary layer in Phoenix, AZ: I. Field observations by long-path DOAS, Atmos. Chem. Phys., 6, 2671–2693, doi:10.5194/acp-6-2671-2006, 2006. 30135, 30136

Wong, K. W. and Stutz, J.: Influence of nocturnal vertical stability on daytime chemistry: A one-dimensional model study, Atmos. Environ., 44, 3753–3760, doi:10.1016/j.atmosenv.2010.06.057, 2010. 30138

Yu, Y., Galle, B., Panday, A., Hodson, E., Prinn, R., and Wang, S.: Observations of high rates of NO_2-HONO conversion in the nocturnal atmospheric boundary layer in Kathmandu, Nepal, Atmos. Chem. Phys., 9, 6401–6415, doi:10.5194/acp-9-6401-2009, 2009. 30145

Ziemba, L. D., Dibb, J. E., Griffin, R. J., Anderson, C. H., Whitlow, S. I., Lefer, B. L., Rappenglück, B., and Flynn, J.: Heterogeneous conversion of nitric acid to nitrous acid on the surface of primary organic aerosol in an urban atmosphere, Atmos. Environ., 44, 4081–4089, doi:10.1016/j.atmosenv.2008.12.024, 2010. 30132, 30145, 30152

ACPD
10, 30129–30170, 2010

Table 1. Observed mixing ratio ranges and detection limits.

	Mixing Ratios	Detection Limits* (Average in parenthesis)	Uncertainty
O_3	0–130 ppb	1–30 ppb (2.5 ppb)	± 3%
NO_2	0.1–60 ppb	0.03–2 ppb (0.12 ppb)	± 5%
HONO	0–2.15 ppb	0.016–0.2 ppb (0.045 ppb)	± 5%

* please note that DOAS calculates an error and detection limit for every absorption spectrum. Detection limits vary with visibility and instrument behavior.

ACPD
10, 30129–30170, 2010

Table 2. Initial concentrations for model simulations.

	1 September	7 September	11 September
O_3	72	67	Low: 9; Mid:15; Up:38
NO_2	10	12	Low: 40; Mid: 37 Up: 7
HONO	0.15	0.13	Low: 0.68; Mid: 0.53 Up: 0.03
SO_2	5	3	3
CO	138	138	138
CH_4	1600	1600	1600
Alkanes	14.95	20.35	15.72
Alkenes	1.92	3.09	5.54
Biogenics	1.3	0.75	0.85
Aromatics	3.49	2.56	24.67
Carbonlys	8.52	8.62	7.55

ACPD
10, 30129–30170, 2010

Table 3. Integrated HONO production and loss over the lowest 300 m throughout the nights of the modeling periods, 1–2 and 7–8 September 2006. Percentage contributions of each process are also shown.

Periods	Production					Loss					Net Prod. [cm^{-2}]
	Ground [%]	Aerosol [%]	Emiss. [%]	NO + OH [%]	Total [cm^{-2}]	Ground [%]	Aerosol [%]	HONO + OH [%]	Vert. Trans. [%]	Total [cm^{-2}]	
1–2 Sep	74	3	17	6	1.7×10^{15}	71	18	1	10	1.4×10^{15}	2.7×10^{14}
7–8 Sep	65	3	21	12	1.8×10^{15}	76	18	1	5	1.3×10^{15}	5.3×10^{14}

ACPD
10, 30129–30170, 2010

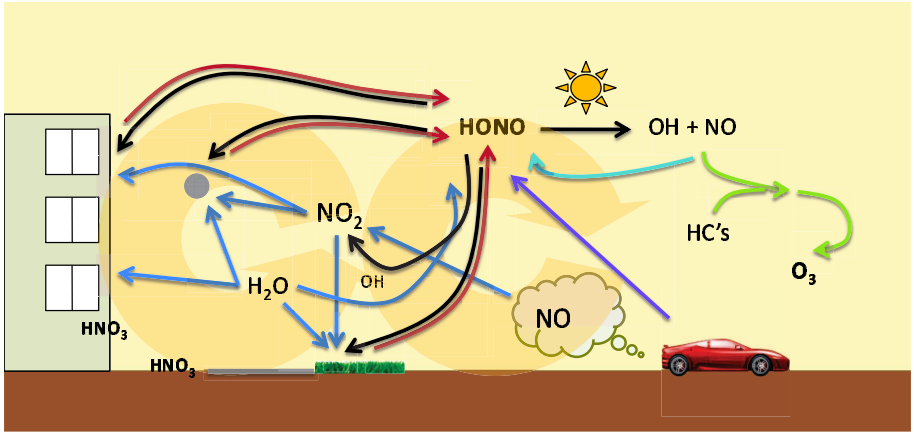

Fig. 1. Schematics of HONO chemistry in urban boundary layer.

ACPD
10, 30129–30170, 2010

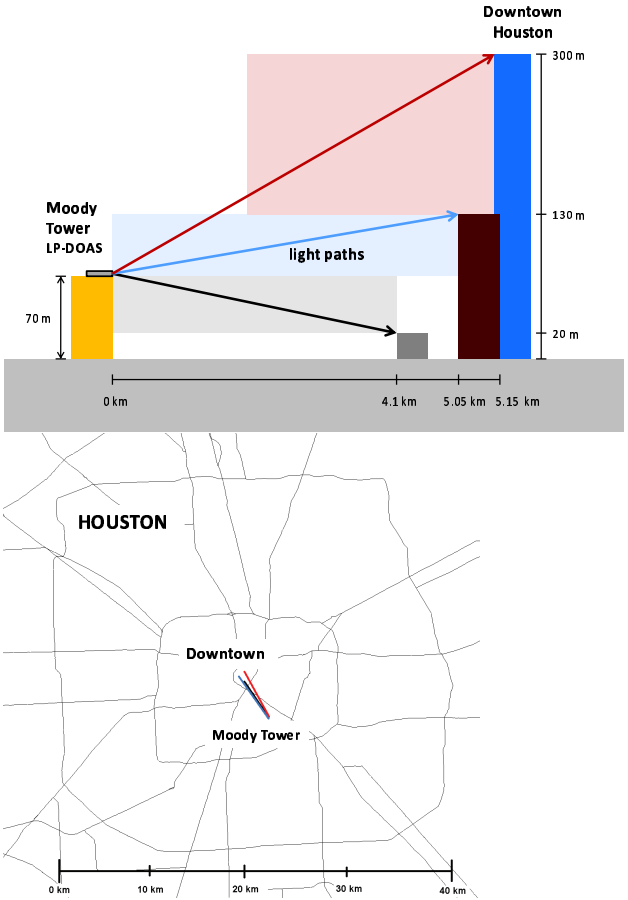

Fig. 2. Light path arrangement of the LP-DOAS systems during TRAMP 2006.

ACPD
10, 30129–30170, 2010

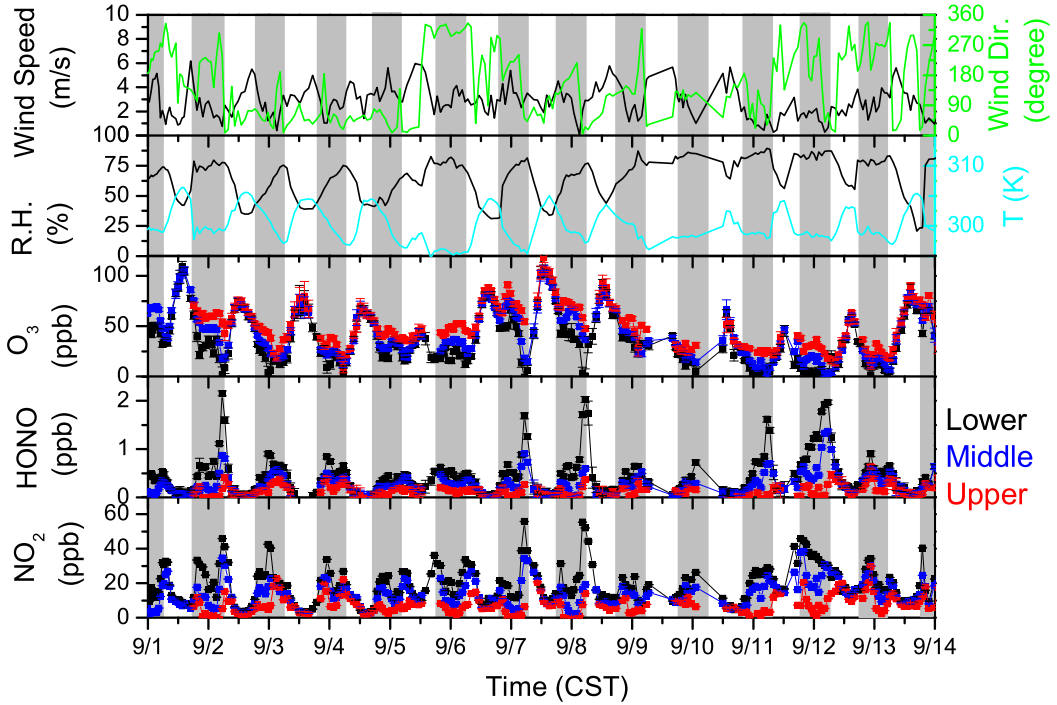

Fig. 3. Overview of LP-DOAS observations of NO_2, HONO and O_3 mixing ratios (lower: 20–70 m, middle: 70–130 m and upper: 130–300 m) from 1–14 September 2006 during TRAMP in Houston, TX. Measurements of R.H. and wind speed and direction at 70 m are also shown.

ACPD
10, 30129–30170, 2010

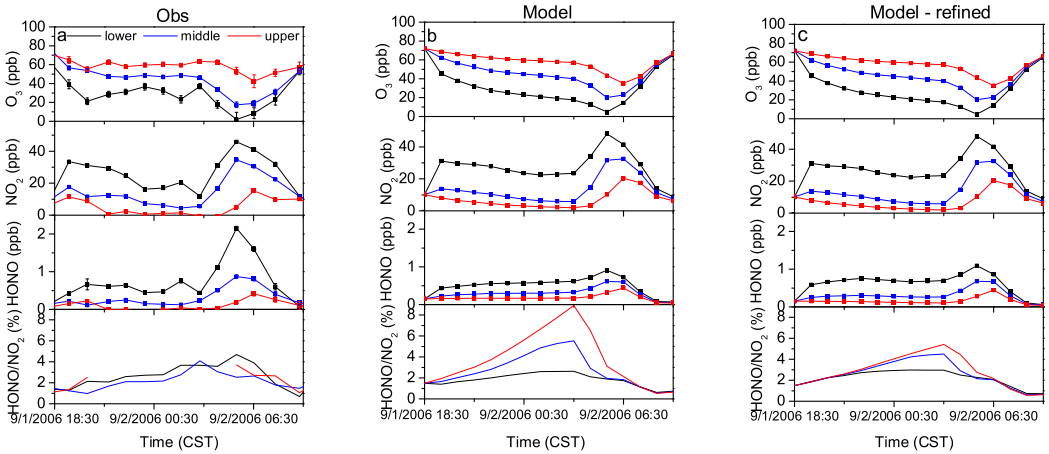

Fig. 4. Comparison of HONO, NO_2, O_3 mixing ratios and HONO to NO_2 ratios between observations (left) and model results (middle and right) on 1–2 September 2006. (Mixing ratios at lower, middle and upper altitudes are plotted in black, blue and red respectively.)

ACPD
10, 30129–30170, 2010

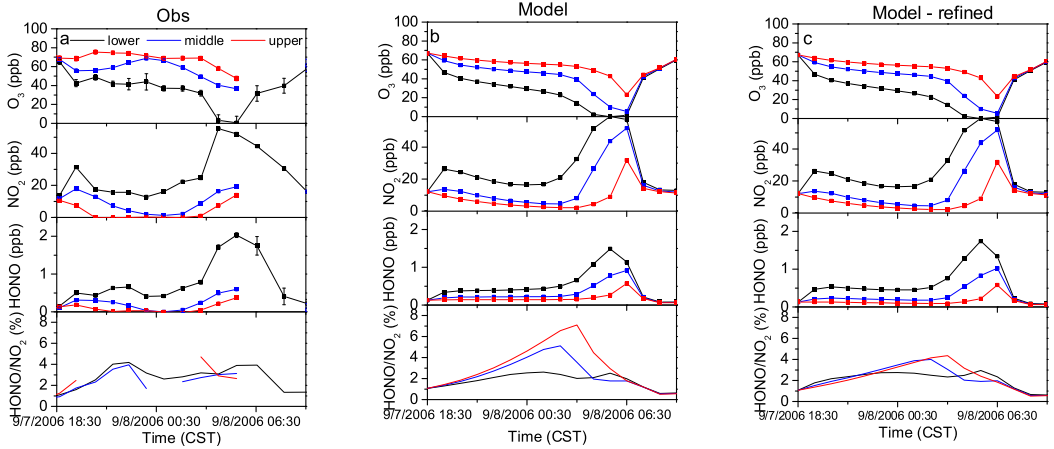

Fig. 5. Comparison of HONO, NO_2, O_3 mixing ratios and HONO to NO_2 ratios between observations (left) and model results (middle and right) on 7–8 September 2006. (Mixing ratios at lower, middle and upper altitudes are plotted in black, blue and red respectively.)

ACPD
10, 30129–30170, 2010

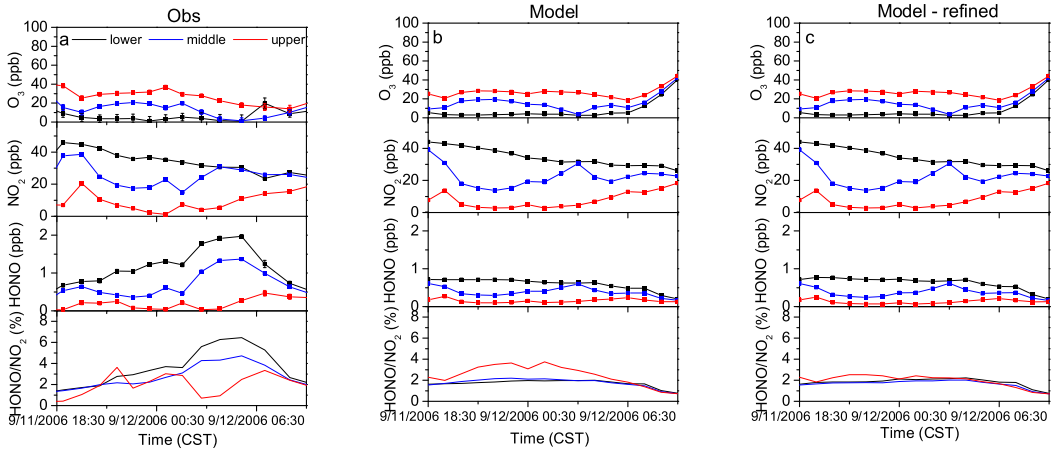

Fig. 6. Comparison of HONO, NO_2, O_3 mixing ratios and HONO/NO_2 between observations (left) and model results (middle and right) on 11–12 September 2006. (Mixing ratios at lower, middle and upper altitudes are plotted in black, blue and red respectively.)

ACPD
10, 30129–30170, 2010

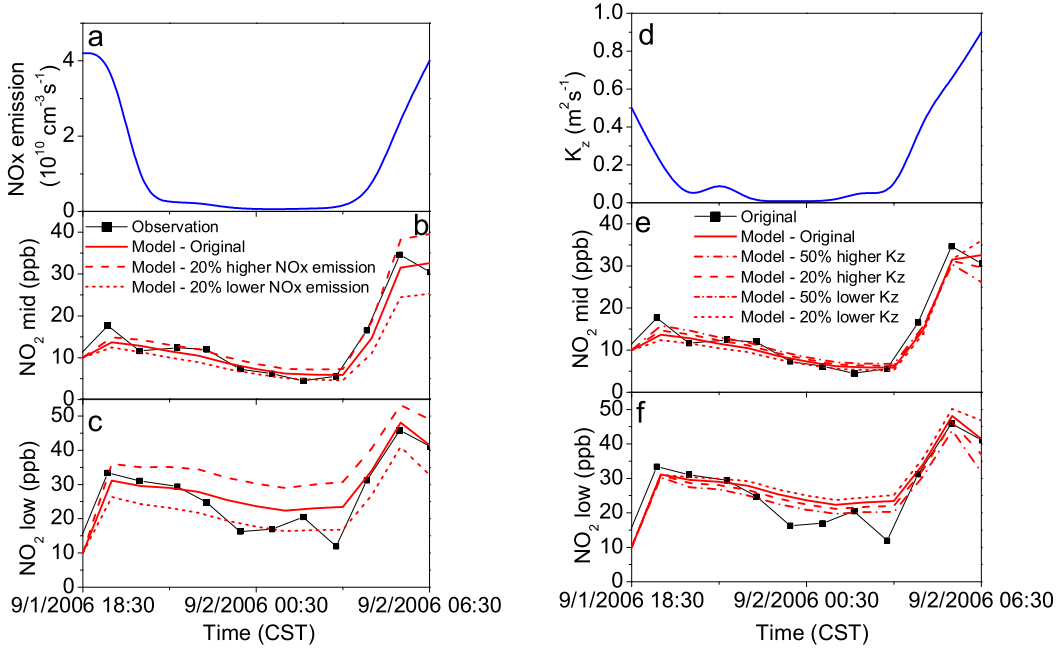

Fig. 7. Sensivity of NO_2 mixing ratios in the lower and middle light paths intervals to change in NO_x emission and eddy diffusivity. NO_x emission and eddy diffusivity at 10 m are plotted as well.

ACPD
10, 30129–30170, 2010

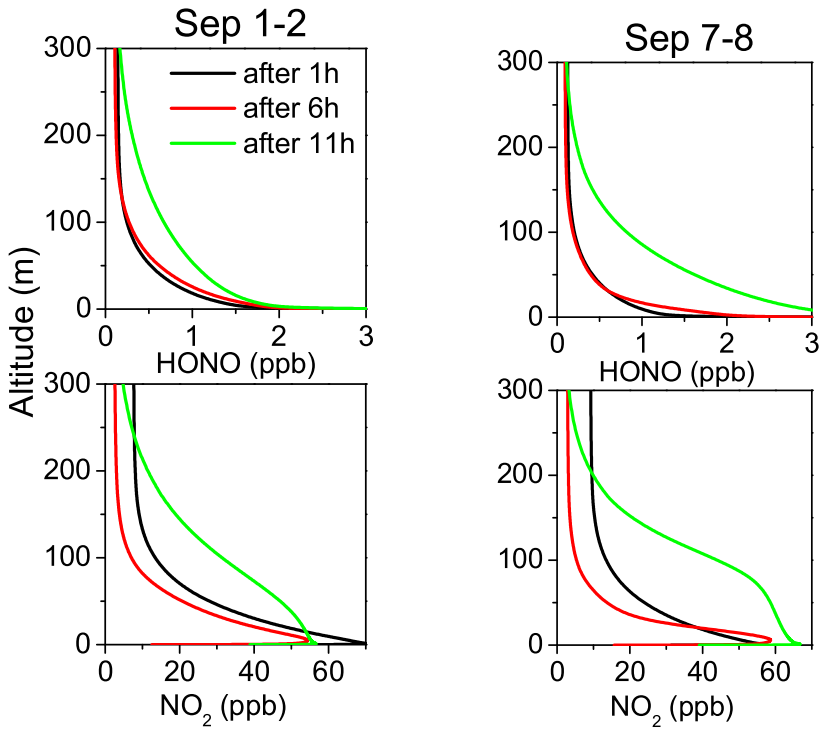

Fig. 8. Vertical profiles of modeled HONO and NO_2 mixing ratios at 19:30, 00:30 and 05:30 CST of 1–2 September (left) and 7–8 September 2006 (right).

ACPD
10, 30129–30170, 2010

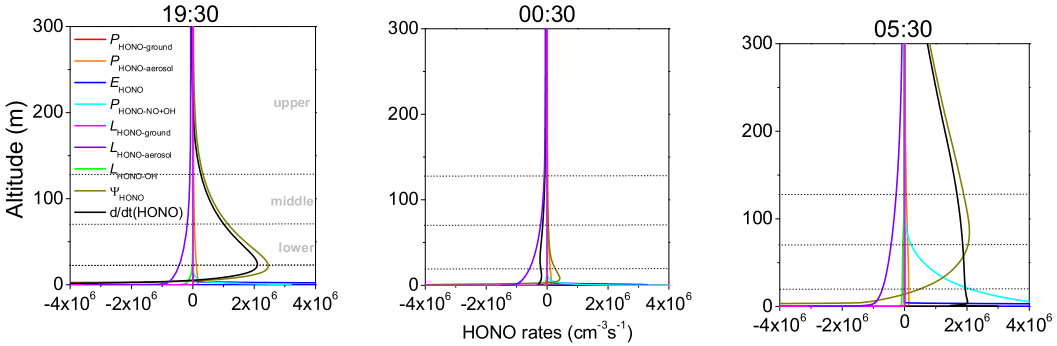

Fig. 9. Modeled vertical profiles of HONO rates at 19:30, 00:30 and 05:30 CST during the night of 1–2 September 2006.

ACPD
10, 30129–30170, 2010

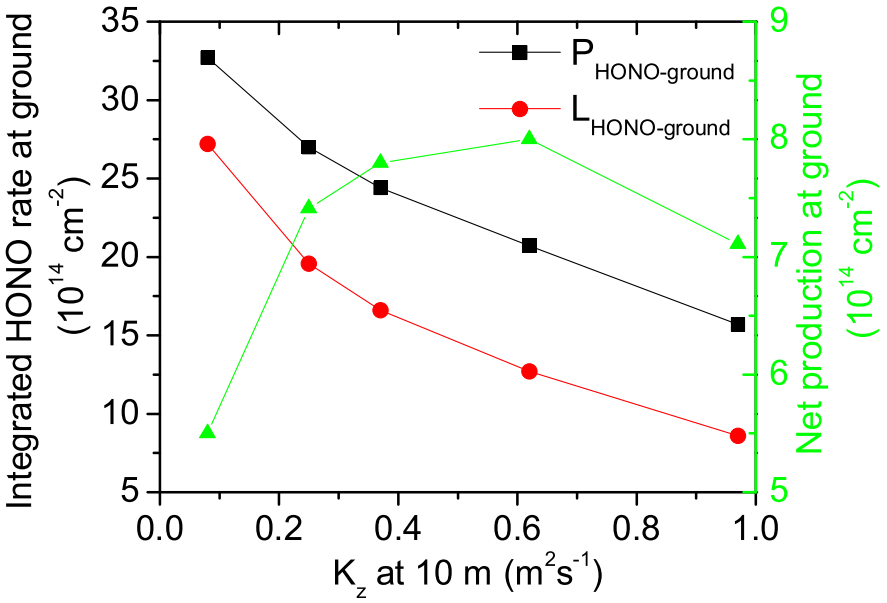

Fig. 10. Sensitivity of integrated HONO formation and loss rates throughout the night at the ground with stability. Eddy diffusivity at 10 m is plotted as a measure of vertical stability.

ACPD
10, 30129–30170, 2010